ADVANCED FUNCTIONAL MATERIALS
www.afm-journal.de

Materials Views
www.MaterialsViews.com

A High-Energy Li-Ion Battery Using a Silicon-Based Anode and a Nano-Structured Layered Composite Cathode

Changju Chae, Hyung-Joo Noh, Jung Kyoo Lee, Bruno Scrosati,* and Yang-Kook Sun**

High capacity electrodes based on a Si composite anode and a layered composite oxide cathode, Ni-rich $Li[Ni_{0.75}Co_{0.1}Mn_{0.15}]O_2$, are evaluated and combined to fabricate a high energy lithium ion battery. The Si composite anode, Si/C-IWGS (internally wired with graphene sheets), is prepared by a scalable sol–gel process. The Si/C-IWGS anode delivers a high capacity of >800 mAh g^{-1} with an excellent cycling stability of up to 200 cycles, mainly due to the small amount of graphene (~6 wt%). The cathode ($Li[Ni_{0.75}Co_{0.1}Mn_{0.15}]O_2$) is structurally optimized (Ni-rich core and a Ni-depleted shell with a continuous concentration gradient between the core and shell, i.e., a full concentration gradient, FCG, cathode) so as to deliver a high capacity (>200 mAh g^{-1}) with excellent stability at high voltage (~4.3 V). A novel lithium ion battery system based on the Si/C-IWGS anode and FCG cathode successfully demonstrates a high energy density (240 Wh kg^{-1} at least) as well as an unprecedented excellent cycling stability of up to 750 cycles between 2.7 and 4.2 V at 1C. As a result, the novel battery system is an attractive candidate for energy storage applications demanding a high energy density and long cycle life.

1. Introduction

Despite recent progress in the performance of lithium-ion batteries (LIBs), their energy density and cycle life still remain as critical challenges for applications in various electrified vehicles.[1–6] Increasing the energy density of LIBs necessitates the development of electrode materials that offer a higher capacity and improved safety.[7,8] Extending the cycle life of LIBs requires the electrochemical stabilization of active electrodes for both cathode and anode materials and their interface with the electrolyte.[8]

The energy density of LIBs can be improved when advanced anode materials are available to replace the graphitic carbon anode whose theoretical capacity is limited to 372 mAh g^{-1}. Promising candidates are lithium metal alloys or transition metal oxides.[9–11] Among them, silicon is an ideal anode material because it offers a low voltage for charging and the highest specific and volumetric capacities ($Li_{15}Si_4 \approx$ 3,579 mAh g^{-1} and 8340 mAh mL^{-1}) among known elements.[12,13] In spite of these highly appealing features, it has long been a critical challenge to design silicon-based electrode materials in a scalable way which maintain their high capacity over prolonged cycling due to both disastrous electrode pulverization due to huge volume variations (~300%)[13] and the instability of solid-electrolyte interface (SEI) layers.[8] Significant progresses have been made recently in addressing these issues and thus, achieving stable cycling performance of Si-based composite electrodes. The highly encouraging results are ascribed to combined contributions from the 1) strategic design of Si-based electrode materials that are effectively releasing or accommodating structural stress,[8,14–25] 2) adoption of new polymeric binders,[13,26–28] and 3) electrolyte additives for the formation of a favorable SEI layer.[21,29–33]

For the cathode side, there have been tremendous research efforts to develop high-capacity cathode materials based on $Li[Ni_{1-x}M_x]O_2$ ($x \leq 0.2$) since they offer a high capacity of 200 mAh g^{-1}.[1,3,6,34] However, these materials suffer from a poor cycle life and thermal characteristics, particularly at elevated temperatures because the reactive and unstable Ni^{4+} ions in the highly delithiated $Li_{1-\delta}[Ni_{1-x}M_x]O_2$ are naturally reduced to form stable $Li_xNi_{1-x}O$ and the concurrently released oxygen from the host structure may lead to thermal runway with the potential of explosion.[35–37] Recently, these issues have been resolved by developing a novel core-shell structured layered lithium metal oxide.[38] The nickel-rich core, $Li[Ni_{0.8}Co_{0.1}Mn_{0.1}]O_2$, delivered a high capacity and the manganese-rich shell, $Li[Ni_{0.5}Mn_{0.5}]O_2$, provided significantly improved thermal and structural stabilities by reducing the reactivity of reactive Ni^{4+} ions with electrolyte. A more advanced cathode to address the

C. Chae, Prof. J. K. Lee
Department of Chemical Engineering
Dong-A University
Busan 604–714, Republic of Korea
E-mail: jklee88@dau.ac.kr
H.-J. Noh, Prof. Y.-K. Sun
Department of Energy Engineering
Hanyang University
Seoul 133–791, Republic of Korea
E-mail: yksun@hanyang.ac.kr
Prof. B. Scrosati
Italian Institute of Technology
Genova, Italy and
King Abdulaziz University
Jeddah, Saudi Arabia
E-mail: bruno.scrosati@gmail.com
Prof. Y.-K. Sun
Chemistry Department
Faculty of Science
King Abdulaziz University
Jeddah 21589, Saudi Arabia

DOI: 10.1002/adfm.201303766

inherent instability issues of the Ni-rich layered cathode was achieved very recently with a novel high capacity full concentration gradient (FCG) material in which the nickel concentration decreases linearly from the center towards the particle surface while the manganese concentration increases gradually.[39] The nickel-rich FCG cathode, whose nominal composition is $LiNi_{0.75}Co_{0.1}Mn_{0.15}O_2$, exhibited a very high capacity (215 mAh g^{-1} at 0.2 C) with more pronounced cycling stability at high voltages and temperatures than previous core-shell materials.[39]

At present, the most promising electrode materials to enhance the energy density of LIBs are silicon-based composites for the anode and layered composite oxides ($LiNi_{1-x}M_xO_2$ (M = transition metal)) for the cathode. When electrodes with a high reliability are combined into a complete Li-ion cell, a high energy LIB can be achieved. A few previous works demonstrated Li-ion full cells by coupling silicon-based anodes with various cathodes such as $LiCoO_2$,[14,40] $Li_{1.2}Ni_{0.2}Mn_{0.6}O_2$,[41] and $LIMn_{1/3}Co_{1/3}Ni_{1/3}O_2$.[42] However, their cycling stabilities were not satisfactory. In this study, a new Si/C nanocomposite internally wired with a small amount of graphene sheets (GS) (hereafter Si/C-IWGS) was prepared by a scalable sol-gel method. In the Si/C-IWGS, GS was ideally dispersed in the composite and played the role of maintaining electrical networks through the electrode against large volume variations during full range cycling between 0.01–1.5 V vs. Li^+/Li. The Si/C-IWGS composite showed a reversible capacity of over 800 mAh g^{-1} at 100 mA g^{-1} and excellent cycling stability for 200 cycles. For this study, the FCG cathode material was further improved in terms of cycling performance by increasing the primary particle size. The modified FCG cathode delivered 210 mAh g^{-1} between 2.7 and 4.3 V vs. Li^+/Li with an excellent capacity retention up to 100 cycles. For further evaluation of electrode materials from a practical viewpoint, it is highly desirable to investigate their electrochemical responses in a full cell configuration. Thus, the Si/C-IWGS anode and FCG cathode were combined in a complete cell to demonstrate a high-energy lithium ion battery with excellent cycling stability. Herein, the detailed electrochemical responses of the Si/C-IWGS anode, FCG cathode, and full Li-ion cell assembled with these electrodes are presented.

2. Results and Discussion

2.1. Anode

Si/C-IWGS was prepared by the readily scalable sol-gel method presented in **Scheme 1**. The whole process was carried out in a one-pot reaction forming a Si-RF-GO composite gel followed by thermal annealing in an inert atmosphere to yield Si/C-IWGS. Since a single graphene sheet has an extremely high surface area with the highest aspect ratio, a small amount is sufficient to internally wire-up the Si/C composite if graphene sheets can be ideally dispersed through the composite. The GO sheets possess oxygen-containing functional groups such as carboxyl, alcohol, and ether, which render the GO suspension stable in various polar solvents including water.[43,44] Furthermore, these highly reactive functional groups in GO can participate in the RF sol-gel reaction in the temperature range of 70–90 °C under slightly basic conditions. Hence, the process should give rise to Si/C-IWGS nanocomposites in which graphene sheets are ideally dispersed to form internal electrical networks through the composite after thermal reduction.

The XRD (X-ray diffraction) patterns of pristine graphite and dried GO paper are shown in Figure S1 (see Supporting Information). The dried GO sample shows a broad X-ray diffraction peak at 2θ values of 10–13° (11.8 Å d-spacing) while the pristine graphite has an intense peak at 2θ = 26.4° (3.4 Å d-spacing) for the graphitic phase. Figure S1b shows a TEM (transmission electron microscopy) image of a wrinkled but very transparent GO sheet. These results support that a well exfoliated and highly dispersed GO aqueous solution was prepared by the modified Hummer's method.

The SEM (scanning electron microscopy) images of the Si/C-IWGS and Si/C are presented in **Figure 1**. Figure 1a shows randomly-shaped particles of Si/C-IWGS but the high magnification image of the edge cross-section in Figure 1b demonstrates the alternating graphene sheets/stacks and carbon-coated Si nanoparticles, while the Si/C composite without GS shows only carbon-coated silicon particulates (Figure 1c,d). The detailed structures of the samples were investigated by TEM. As shown in **Figure 2**, every single Si nanoparticle is embedded in R-F carbon to form a Si/C composite. In the TEM images of the Si/C-IWGS sample (Figure 2a,b), silicon nanoparticles are encapsulated in R-F carbon and the Si/C particles are in intimate contact with the graphene sheets underneath. It was also found that the surfaces of the Si nanoparticles are covered by a thin layer of silicon oxides (mostly SiO_2) (see HRTEM image in Figure S2a) due to partial surface oxidation under the slightly basic conditions of the sol-gel process, which was further confirmed by the XPS (X-ray photoelectron spectroscopy) spectra shown in Figure S2b.

In the XRD patterns of Si/C and Si/C-IWGS shown in Figure S2c, a broad hump at 2θ = 10–25° is observed corresponding to an amorphous carbon phase with the crystalline Si diffraction peaks at 2θ = 28.6°, 47.5°, and 56.3° corresponding

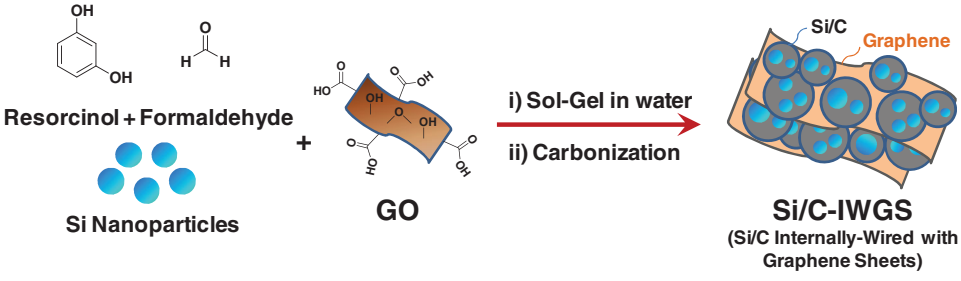

Scheme 1. Schematic diagram of the prepration of Si/C-IWGS.

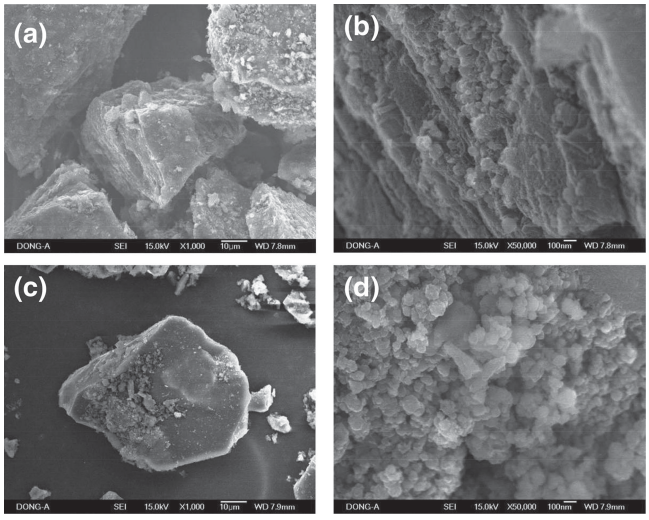

Figure 1. SEM images of (a,b) Si/C-IWGS and (c,d) Si/C.

to the (111), (220), and (311) planes, respectively. In the Si-graphene composites[24,25,45] in which graphene is employed as the sole carbon in relatively high content, the reconstituted graphitic phase is formed where graphene sheets stack and is primarily observed at $2\theta = 26.4°$ with a relatively high intensity. However, the reconstituted graphitic phase is not observed in the XRD pattern of Si/C-IWGS partly due to the very low content of graphene (~6 wt%, see below) in the composite as well as the highly dispersed graphene sheets in the composite without forming thick graphene stacks of a graphitic phase. The Si/SiO_2 contents of both Si/C and Si/C-IWGS were determined to be about 46 wt% from the TGA profile obtained under air shown in Figure S2d. In the total carbon content of 54 wt%, the graphene portion was estimated from the TGA results of GO run under N_2 shown in Figure S2d. The major mass loss occurs at ~200 °C followed by a slow decrease up to 800 °C due to the thermal reduction of GO, i.e., thermal decomposition of oxygen-containing functional groups in GO. The remained mass fraction at 800 °C, i.e., 50 wt% of GO, is assumed to be GS. Hence, considering the initial GO amount in the Si-RF-GO gel, the content of graphene sheets in the Si/C-IWGS nanocomposite was estimated to be around 6 wt%.

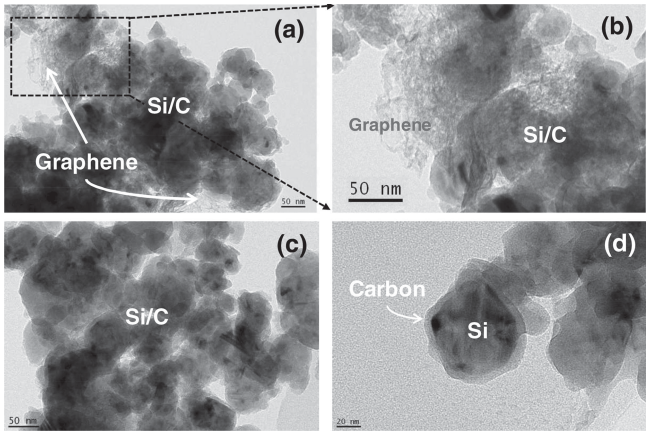

Figure 2. TEM images of (a,b) Si/C-IWGS and (c,d) Si/C.

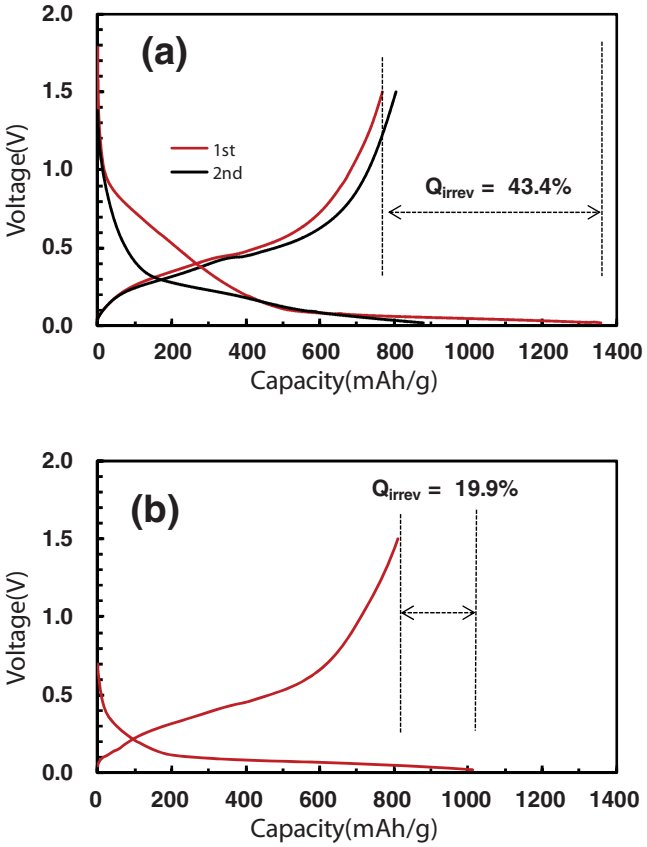

Figure 3. Voltage profiles of (a) Si/C-IWGS and (b) pretreated Si/C-IWGS cycled between 0.02–1.5 V at 100 mA g^{-1}.

The fundamental electrochemical properties of the Si/C-IWGS anode were tested using a 2032 coin-type half-cell, employing Li metal as the anode. The charge/discharge voltage profile of the Si/C-IWGS anode cycled between 0.02–1.5 V at 100 mA g^{-1} is given in **Figure 3**a. In the first discharge, a voltage slope between 1.0–0.2 V appeared due to the well-known solid-electrolyte interface (SEI) film formation and surface oxide layer decomposition, followed by a long voltage plateau between 0.2–0.02 V due to the full lithiation of Si. The first discharge and charge capacities were 1,358 and 768 mAh g^{-1}, respectively, resulting in a coulombic efficiency (CE) of 56.6%. In the second discharge profile, the voltage slope observed between 1.0–0.2 V in the first discharge mostly disappeared, which indicates the electrochemical irreversibility of the SEI formation and Li_2O formation from the oxide layer of Si nanoparticles.[46] The reversible discharge capacity after the first cycle was about 879 mAh g^{-1} at 100 mA g^{-1}. After the surface treatment, the large irreversible capacity loss (Q_{irrev} = 43.4%) was reduced to less than 20% (Figure 3b) while the reversible capacity was maintained above 800 mAh g^{-1}. Hence, the Si/C-IWGS possesses an acceptable range of irreversible capacity loss in the first cycle for assembly into a full cell with a specific cathode.

Figure 4 presents the cycling performances of the Si/C and the Si/C-IWGS composites at various current rates. The Si/C exhibited reversible discharge capacities of 865 and 600 mAh g^{-1} at currents of 100 and 500 mA g^{-1}, respectively. However, the capacity of Si/C at 500 mA g^{-1} started to fade

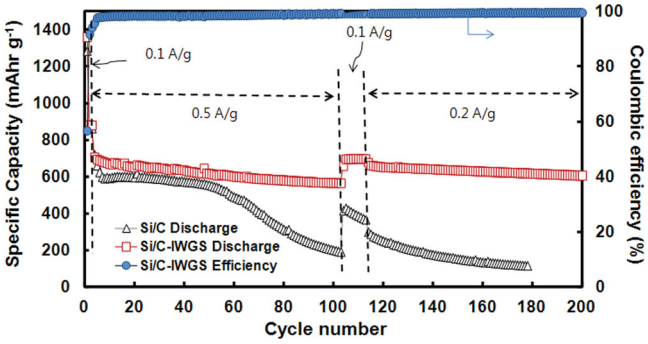

Figure 4. Cycling performances of Si/C and Si/C-IWGS cycled between 0.02–1.5 V.

beginning at the 50th cycle and lost most of its capacity after 100 cycles. The reversible discharge capacity of Si/C-IWGS at 100 mA g^{-1} was about 880 mAh g^{-1} for the initial three cycles. At a current of 500 mA g^{-1}, the discharge capacity was on the order of 700 mAh g^{-1} and the capacity retention after 100 cycles was 82.8% (about 0.18% capacity fading per cycle). After further cycling up to 200 cycles at 200 mA g^{-1}, the capacity retention was 91.9% for 100 cycles (about 0.09% capacity fading per cycle). The CE increased to >97% beyond the fifth cycle. Hence, the Si/C-IWGS anode exhibited excellent cycling stability up to 200 cycles. The enhanced cycleability of Si/C-IWGS compared to that of Si/C could be ascribed to the small amount (~6 wt%) of graphene sheets, which helps to maintain the electrical network through the Si/C composites against the large volume variation experienced during the prolonged charge/discharge processes.

2.2. Cathode

The powder X-ray diffraction (XRD) patterns of FCG $Li[Ni_{0.75}Co_{0.1}Mn_{0.15}]O_2$ in **Figure 5**a confirm the well-crystallized layer structure based on a hexagonal a-$NaFeO_2$ structure with a $R\bar{3}m$ space group and no impurity phases. The lattice parameters were calculated from the XRD pattern using a least squares method based on the $R\bar{3}m$ space group. The lattice parameters for the FCG $Li[Ni_{0.75}Co_{0.1}Mn_{0.15}]O_2$ material are a = 2.871(9) Å and c = 14.210(2) Å, which are slightly lower than the values of $Li[Ni_{0.8}Co_{0.1}Mn_{0.1}]O_2$ (a = 2.879 Å and c = 14.262 Å). The synthesized FCG $Li[Ni_{0.75}Co_{0.1}Mn_{0.15}]O_2$ powders had a spherical morphology with an average particle diameters of about 12 µm (Figure S3). The compositional change within a particle was determined by electron probe X-ray micro-analysis (EPMA) with a probe diameter of 100 nm. As can be seen in Figure 5b, the nickel concentration decreased linearly from 85 at% to 72 at% toward the particle surface, whereas the Mn concentration increased from 5 at% to 17 at%. The Co concentration remained constant from the center to the outer surface of the particle. Figure 5c shows a cross-sectional transmission electron microscopy (TEM) image of a center region of a single FCG particle and the corresponding elemental distributions of Ni, Co, and Mn (by energy-dispersive X-ray spectroscopy (EDS) mapping). As expected, the elemental mapping of Co shows a uniform contrast. On the other hand, nickel was enriched at the particle center and became gradually depleted toward the particle surface, whereas the opposite concentration gradient was observed for manganese. Figure 5d shows a transmission electron microscopy (TEM) image of a single FCG $Li[Ni_{0.75}Co_{0.1}Mn_{0.15}]O_2$ particle that was sectioned by a focused ion beam. Contrary to previously reported results,[39] the FCG secondary powder was composed of long rod-shaped primary particles with lengths reaching 1.2 µm (width ~ 100 nm), aligned to a specific particle center, which is very similar to the morphology reported recently.[47] This unique morphology may give rise to improved cycle life and safety because of the reduced exposed surface area to the electrolyte.

The electrochemical responses of the FCG $Li[Ni_{0.75}Co_{0.1}Mn_{0.15}]O_2$ cathode cycled between 2.7–4.3 V are shown in **Figure 6**. The electrolyte containing FEC was employed to form a more stable SEI layer[29,32] for the Si/C-IWGS anode. Therefore, the FCG cathode was also tested by using the same electrolyte. FCG $Li[Ni_{0.75}Co_{0.1}Mn_{0.15}]O_2$ without FEC in the electrolyte delivered an initial discharge capacity of 210 mAh g^{-1} at a 0.1 C rate as well as a high Coulombic efficiency of 94.7%. For the FCG tested with the electrolyte containing FEC, the initial capacity and Coulombic efficiency decreased slightly to 197.3 mAh g^{-1} and 92.1%, respectively (Figure 5a). However, the capacity retention at 0.5 C after 100 cycles improved

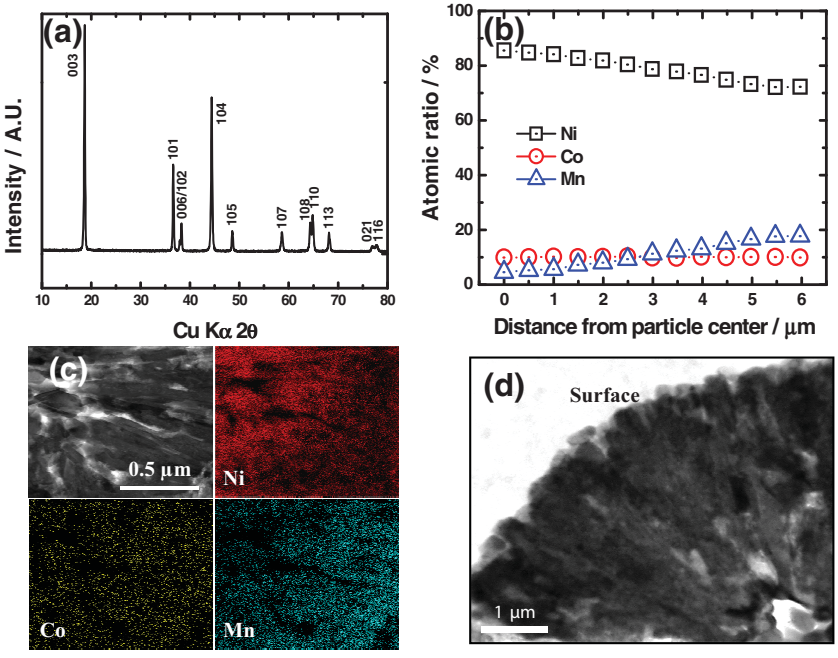

Figure 5. (a) XRD pattern of the FCG $Li[Ni_{0.75}Co_{0.1}Mn_{0.15}]O_2$ powders, (b) EPMA line scan of the integrated atomic ratio of transition metals as a function of the distance from the particle center to the surface for a single FCG $Li[Ni_{0.75}Co_{0.1}Mn_{0.15}]O_2$ particle, (c) cross-sectional TEM and EDS mapping of Ni, Co, and Mn at the particle center region, and (d) cross-sectional TEM image of a single FCG $Li[Ni_{0.75}Co_{0.1}Mn_{0.15}]O_2$ particle.

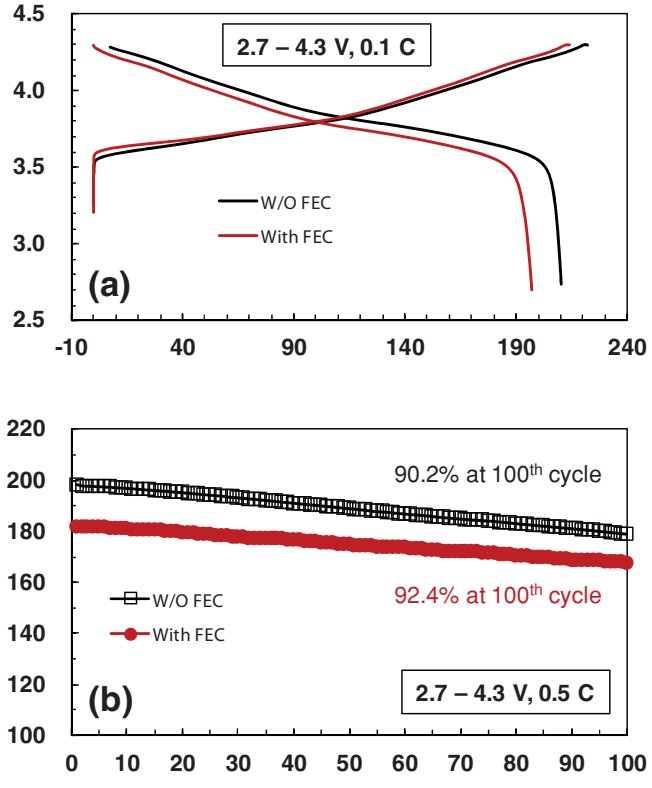

Figure 6. (a) Voltage profiles of the FCG cathode cycled at a 0.1 C rate and the (b) cycling performance of the FCG cathode cycled at a 0.5 C rate between 2.7 and 4.3 V.

slightly from 90.2% to 92.4% for the FEC containing electrolyte (Figure 6b). An enhanced cycling stability with FEC containing electrolyte was also reported for $LiMn_2O_4$ and $LiFePO_4$ electrodes.[48,49] Overall, the FEC exerts no detrimental influence on the performance of the FCG cathode while it helps in the formation of a more stable SEI layer on a Si-based anode.

2.3. Complete Li-Ion Cell: Si/C-IWGS Anode and FCG $Li[Ni_{0.75}Co_{0.1}Mn_{0.15}]O_2$ Cathode

Finally, the pretreated Si/C-IWGS (Figure 3b) anode was combined with the FCG $Li[Ni_{0.75}Co_{0.1}Mn_{0.15}]O_2$ cathode to form a complete Li-ion battery. **Figure 7** shows a typical charge/discharge voltage profile cycled between 2.7–4.2 V at a 0.1 C rate with respect to the cathode. The first charge and discharge capacities were 206 and 196 mAh g^{-1}, respectively, yielding a CE as high as 95%. The practical working voltage of the battery is in the range of 3.2–4.2 V, on average, and the specific capacity per cathode mass is on the order of 200 mAh g^{-1}. Therefore, a specific energy density of 720 Wh kg^{-1} can be obtained if the average working voltage of the battery is assumed to be 3.6 V. By assuming a 1/3 reduction factor (which is applicable for LIBs using a graphite anode) to account for the weight of the electrolyte, current collector, and aluminum case,[6] a practical specific energy density of 240 Wh kg^{-1} is obtained. Considering the additional gain of the specific energy due to the mass reduction of the anode material by using high capacity Si/C-IWGS

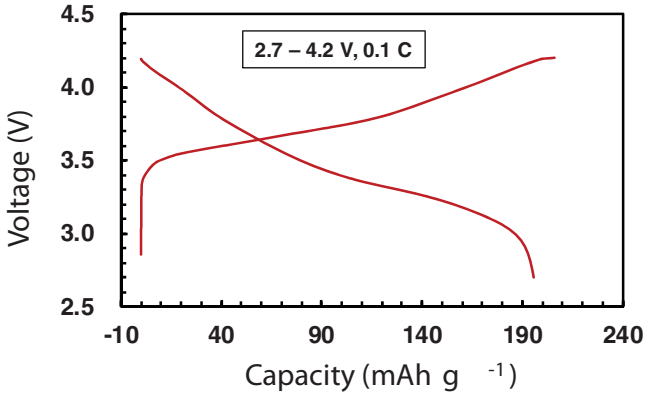

Figure 7. Voltage profile of the lithium ion battery based on the Si/C-IWGS anode and FCG cathode cycled between 2.7 and 4.2 V at a 0.1 C rate.

(880 mAh/g for Si/C-IWGS vs. 372 mAh/g for graphite), the cell can provide a specific energy density greater than 240 Wh kg^{-1}. Thus, the battery comprised of the Si/C-IWGS anode and the FCG cathode can offer an energy density far beyond those offered by current LIBs (~150 Wh kg^{-1}).[3] The enhanced volumetric capacity is another benefit of the high capacity anode.

Figure 8 presents the cycling performance of the battery cycled between 2.7 and 4.2 V. The first and second cycles were conducted at 0.1 C and 0.5 C rates and the corresponding discharge capacities were 196 and 180 mAh g^{-1}, respectively. From the third cycle on, the battery was cycled at 1 C for up to 750 cycles. The discharge capacity at 1 C was 170 mAh g^{-1} and the battery still delivered 88.4% of the initial capacity after 750 cycles (about 0.016% capacity fading per cycle), demonstrating the excellent cycling stability of the novel battery system based on the Si/C-IWGS anode and FCG cathode. To the best of our knowledge, the battery system containing Si/C-IWGS and FCG electrodes can offer superior performances in terms of energy density and cycling life compared to those reported in the literature.[6,33,40–42] The high CE values beyond the third cycle (>98.5%) also demonstrates the high round-trip efficiency of the battery system.

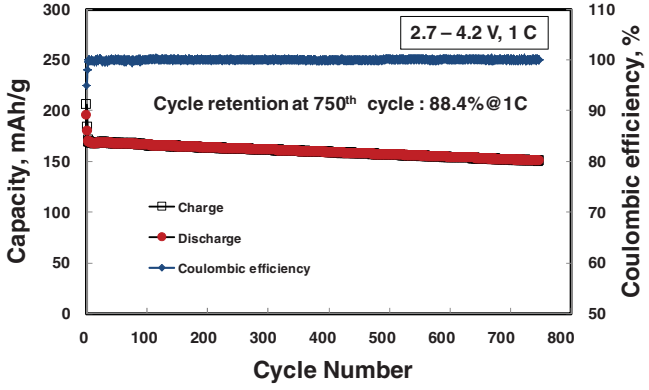

Figure 8. Cycling performance of the lithium ion battery based on the Si/C-IWGS anode and FCG cathode cycled between 2.7 and 4.2 V at a 1.0 C rate.

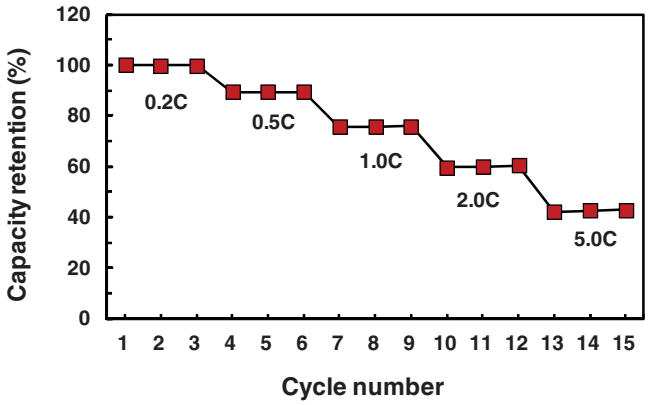

Figure 9. Rate responses of lithium ion battery based on the Si/C-IWGS anode and FCG cathode cycled between 2.7 and 4.2 V.

Figure 9 shows the rate response of the battery. Relative to the capacity at 0.2 C, the battery delivered about 90, 76, and 60% at 0.5, 1.0, and 2.0 C rates, respectively. At 5 C, the capacity retention was 42%. Hence, the electrochemical responses obtained in this study demonstrate an advanced battery system with high energy density, high rate capability as well as a long cycle life.

3. Conclusions

A scalable sol–gel process was successfully demonstrated for the preparation of Si/C-IWGS in which graphene sheets were ideally dispersed to make efficient electrical networks in the composite. A small amount of graphene (~6 wt%) was quite effective in achieving stable cycling of a Si-based carbon composite against large volume changes. The Si/C-IWGS anode was combined with a high performance FCG cathode ($LiNi_{0.75}Co_{0.1}Mn_{0.15}O_2$) which was structurally optimized (Ni-rich center, Mn-rich shell, and a continuous concentration gradient between the center and surface) to deliver a high capacity with excellent stability. Thus, the obtained novel Li-ion battery system successfully demonstrated a high energy density (240 Wh kg^{-1} at least) as well as an unprecedented excellent cycling stability up to 750 cycles between 2.7 and 4.2 V at 1 C. It is quite convincing that the novel battery system based on the Si/C-IWGS anode and FCG cathode can be an attractive candidate for energy storage applications demanding a high energy density and long cycle life.

4. Experimental Section

4.1. Preparation of Electrode Materials

Anode Material: The graphene oxide (GO) was prepared by a modified Hummers method[24,50] using commercial flake graphite (Asbury Carbons, 230U Grade, High Carbon Natural Graphite 99+). GO was diluted to make a ~6% w/w solution in DI water and was subjected to ultra-sonication to obtain an aqueous dispersion of GO sheets which was stored in the dark.To prepare the Si/C-IWGS anode material, Si nanoparticles (50 nm, KCC Corp. Ltd., Korea) were dispersed in DI water (70 mL per g Si) in a flask with sonication. To this dispersion, a specific amount of the GO solution (corresponding to 0.37 wt% of GO in the mixture) was added and the mixture was subjected to sonication to obtain a homogeneous dispersion. To the mixture, resorcinol (**R**, 2.2 g per g Si) and formaldehyde (**F**, 37 wt% in H_2O, 3.4 mL per g Si) were added followed by sodium carbonate (2.0 mL of 0.2 M solution per g Si) under stirring. The mixture was stirred for 1 h at RT and heated at 70 °C in a sealed flask under stirring until the whole mixture formed a gel. The composite gel was further aged at 90 °C overnight for further cross-linking of the gel clusters. The composite gel was thoroughly washed and filtered three times with water to remove the catalyst. Subsequently, three solvent exchanges with 70 mL of isopropanol were carried out. After filtering, the gel was dried in air at 80 °C overnight. The dried composite gel was heated in a tube furnace under 100 mL min^{-1} of flowing Ar (99.999%) to 850 °C at a ramp rate of 5 °C/min and maintained at 850 °C for 2 h to obtain the Si/C-IWGS nanocomposite. As a reference electrode, a Si/C composite was prepared by following the same procedure but without the addition of GO in the gel solution.

Cathode Material: The FCG, $Li[Ni_{0.75}Co_{0.1}Mn_{0.15}]O_2$, was prepared by a coprecipitation method similar to that described previously,[39] which was modified by increasing the concentration of ammonium hydroxide (molar ratio of ammonium hydroxide to transition metal = 1.0) and sodium hydroxide (molar ratio of sodium hydroxide to transition metal = 2.0). A Ni-poor aqueous solution (Ni:Co:Mn molar ratio of 0.64:10:26) from tank 2 comprised of $NiSO_4{\cdot}6H_2O$, $CoSO_4{\cdot}7H_2O$, and $MnSO_4{\cdot}5H_2O$ was slowly pumped into a Ni-rich (Ni:Co:Mn = 0.9:0.1:0.0 in molar ratio) stock solution in tank 1, after which the homogeneously mixed solution was fed into a continuously stirred tank reactor (CSTR). The obtained FCG $[Ni_{0.75}Co_{0.1}Mn_{0.15}](OH)_2$ hydroxide precursor was mixed with $LiOH{\cdot}H_2O$ (Li/(Ni+Co+Mn) = 1 molar ratio) and calcined at 780 °C for 15 h in air.

4.2. Characterizations

Materials Characterizations: Powder X-ray diffraction (XRD) patterns of the samples were recorded on an Ultima IV, Rigaku model D/MAX-50 kV system (Cu-Kα radiation, λ = 1.5418 Å). The morphologies of the samples were investigated using field-emission scanning electron microscopy (FE-SEM, JEOL JSM-35CF operated at 10 kV) and transmission electron microscopy (TEM, JEOL JEM-2010 operated at 200 kV). The carbon contents in Si/C and Si/C-IWGS were determined by the weight loss obtained from the thermogravimetric analysis (TGA) which was performed up to a temperature of 800°C at a ramp rate of 10 °C min^{-1} under air flow. The graphene content in the Si/C-IWGS was determined by the TGA results of the dried GO run under N_2 flow. X-ray photoelectron spectroscopy (XPS) was conducted with a Thermo Electron Corporation spectrometer. To investigate the compositional changes of Ni, Co, and Mn throughout an entire single FCG $Li[Ni_{0.75}Co_{0.1}Mn_{0.15}]O_2$ particle, cross-sections of the particles were prepared by embedding the particles in an epoxy and grinding them flat. Line scans of the polished surfaces for the prepared FCG $Li[Ni_{0.75}Co_{0.1}Mn_{0.15}]O_2$ powders were analyzed via electron probe microanalysis (EPMA) (JEOL, Model JXA-8100).

Electrochemical Responses - Anode: Electrochemical tests were performed using CR2032 coin cells with Li foil as the counter electrode. The working electrode of Si/C-IWGS was prepared by casting a paste that consisted of 80 wt% active material (Si/C-IWGS), 10 wt% conductive additive (Super P Li, Timcal Ltd.), and 10 wt% polyvinyl alcohol (PVA)[28] binder dissolved in anhydrous dimethyl sulfoxide onto a copper foil using a Meyer-Bar coating device (Kipae E&T, Korea). The coated electrodes were roll-pressed and then vacuum dried at 80 °C for 12 h. The resulting electrode thickness was about 30–40 μm. A Celgard 2400 polypropylene membrane (25 μm thick) was used as the separator. 1.2 M $LiPF_6$ in an ethylene carbonate-ethyl methyl carbonate (3:7 in volume, PANAX ETEC Co., Ltd, Korea) containing 10 vol% (12.8 wt%) fluoroethylene carbonate (FEC) was used as the electrolyte. The cells were cycled on a galvanostat (WonATech Co., Ltd., Korea) over the voltage range of 1.5–0.02 V vs. Li^+/Li.

Electrochemical Responses - Cathode: For fabrication of the cathodes, the prepared powders were mixed with carbon black and polyvinylidene fluoride (85:7.5:7.5 in weight) in N-methylpyrrolidinon. The obtained slurry was coated onto Al foil and roll-pressed. The electrodes were dried overnight at 120°C in a vacuum before use. Preliminary cell tests were performed using a 2032 coin-type cell using Li metal as the anode. The electrolyte solution was 1.2 M $LiPF_6$ in ethylene carbonate-

ethyl methyl carbonate (3:7 in volume, PANAX ETEC Co., Ltd, Korea) containing 10 vol% fluoroethylene carbonate (FEC). The cells were cycled galvanostatically between 2.7 and 4.3 V.

Electrochemical Responses - Complete Li-ion Cells: Before completing the Li-ion cell assembly, the Si/C-IWGS electrode was placed in direct contact with a Li foil by the electrolyte solution for 60 min in order to suppress the first irreversible capacity loss.[6] The FCG cathode and pretreated Si/C-IWGS anode electrodes were assembled in CR2032 coin cells with an N/P ratio of 1.2 using the same separator and electrolyte as those used in the half-cell test. The cell was cathode limited and was charged and discharged between 2.7 and 4.2 V by applying a constant 1 C current (corresponding to 200 mA g^{-1} based on the weight of cathode active material) at 25 °C, otherwise notified on a TOSCAT-3100U (TOYO SYSTEM Co., JAPAN).

Supporting Information

Supporting Information is available from the Wiley Online Library or from the author.

Acknowledgements

C. Chae and H.-J. Noh contributed equally to this work. This work was supported by grants from the National Research Foundation of Korea funded by the Korean Government (MEST) (NRF-2009-C1AAA001–0093307) and by the Human Resources Development program (No. 20124010203310) of the Korea Institute of Energy Technology Evaluation of Planning (KETEP) grant funded by the Korea Government Ministry of Trade, Industry and Energy.

Received: November 6, 2013
Published online: February 12, 2014

[1] B. Scrosati, J. Garche, *J. Power Sources* **2010**, *195*, 2419.
[2] B. Scrosati, J. Hassoun, Y. K. Sun, *Energy Environ. Sci.* **2011**, *4*, 3287.
[3] M. M. Thackeray, C. Wolverton, E. D. Isaacs, *Energy Environ. Sci.* **2012**, *5*, 7854.
[4] J. M. Tarascon, *Philos. Trans. R. Soc. A-Math. Phys. Eng. Sci.* **2010**, *368*, 3227.
[5] J. M. Tarascon, M. Armand, *Nature* **2001**, *414*, 359.
[6] J. Hassoun, K. S. Lee, Y. K. Sun, B. Scrosati, *J. Am. Chem. Soc.* **2011**, *133*, 3139.
[7] M. S. Whittingham, *Chem. Rev.* **2004**, *104*, 4271.
[8] H. Wu, G. Chan, J. W. Choi, I. Ryu, Y. Yao, M. T. McDowell, S. W. Lee, A. Jackson, Y. Yang, L. B. Hu, Y. Cui, *Nat. Nanotechnol.* **2012**, *7*, 309.
[9] R. A. Huggins, *J. Power Sources* **1999**, *82*, 13.
[10] B. Gao, S. Sinha, L. Fleming, O. Zhou, *Adv. Mater.* **2001**, *13*, 816.
[11] P. Poizot, S. Laruelle, S. Grugeon, L. Dupont, J. M. Tarascon, *Nature* **2000**, *407*, 496.
[12] M. N. Obrovac, L. Christensen, *Electrochem. Solid-State Lett.* **2004**, *7*, A93.
[13] S. D. Beattie, D. Larcher, M. Morcrette, B. Simon, J. M. Tarascon, *J. Electrochem. Soc.* **2008**, *155*, A158.
[14] M. H. Park, M. G. Kim, J. Joo, K. Kim, J. Kim, S. Ahn, Y. Cui, J. Cho, *Nano Lett.* **2009**, *9*, 3844.
[15] A. Magasinski, P. Dixon, B. Hertzberg, A. Kvit, J. Ayala, G. Yushin, *Nat. Mater.* **2010**, *9*, 461.
[16] H. Wu, G. Y. Zheng, N. A. Liu, T. J. Carney, Y. Yang, Y. Cui, *Nano Lett.* **2012**, *12*, 904.
[17] N. Liu, H. Wu, M. T. McDowell, Y. Yao, C. M. Wang, Y. Cui, *Nano Lett.* **2012**, *12*, 3315.
[18] S. R. Chen, M. L. Gordin, R. Yi, G. Howlett, H. Sohn, D. H. Wang, *Phys. Chem. Chem. Phys.* **2012**, *14*, 12741.
[19] J. Q. Wang, Y. Yu, L. Gu, C. L. Wang, K. Tang, J. Maier, *Nanoscale* **2013**, *5*, 2647.
[20] J. K. Lee, M. C. Kung, L. Trahey, M. N. Missaghi, H. H. Kung, *Chem. Mater.* **2009**, *21*, 6.
[21] Y. S. Hu, R. Demir-Cakan, M. M. Titirici, J. O. Muller, R. Schlogl, M. Antonietti, J. Maier, *Angew. Chem. Int. Ed.* **2008**, *47*, 1645.
[22] J. H. Lee, W. J. Kim, J. Y. Kim, S. H. Lim, S. M. Lee, *J. Power Sources* **2008**, *176*, 353.
[23] H. Kim, B. Han, J. Choo, J. Cho, *Angew. Chem. Int. Ed.* **2008**, *47*, 10151.
[24] J. K. Lee, K. B. Smith, C. M. Hayner, H. H. Kung, *Chem. Commun.* **2010**, *46*, 2025.
[25] X. Zhao, C. M. Hayner, M. C. Kung, H. H. Kung, *Adv. Energy Mater.* **2011**, *1*, 1079.
[26] G. Liu, S. D. Xun, N. Vukmirovic, X. Y. Song, P. Olalde-Velasco, H. H. Zheng, V. S. Battaglia, L. W. Wang, W. L. Yang, *Adv. Mater.* **2011**, *23*, 4679.
[27] A. Magasinski, B. Zdyrko, I. Kovalenko, B. Hertzberg, R. Burtovyy, C. F. Huebner, T. F. Fuller, I. Luzinov, G. Yushin, *ACS Appl. Mater. Inter.* **2011**, *2*, 3004.
[28] H. K. Park, B. S. Kong, E. S. Oh, *Electrochem. Commun.* **2011**, *13*, 1051.
[29] H. Nakai, T. Kubota, A. Kita, A. Kawashima, *J. Electrochem. Soc.* **2011**, *158*, A798.
[30] D. Aurbach, K. Gamolsky, B. Markovsky, Y. Gofer, M. Schmidt, U. Heider, *Electrochim. Acta* **2002**, *47*, 1423.
[31] R. McMillan, H. Slegr, Z. X. Shu, W. D. Wang, *J. Power Sources* **1999**, *81*, 20.
[32] N. S. Choi, K. H. Yew, K. Y. Lee, M. Sung, H. Kim, S. S. Kim, *J. Power Sources* **2006**, *161*, 1254.
[33] R. Elazari, G. Salitra, G. Gershinsky, A. Garsuch, A. Panchenko, D. Aurbach, *J. Electrochem. Soc.* **2012**, *159*, A1440.
[34] C. Liu, F. Li, L. P. Ma, H. M. Cheng, *Adv. Mater.* **2010**, *22*, E28.
[35] S. O. H. Arai, Y. Sakurai, J. Yamaki, *Solid State Ionics* **1998**, *109*, 295.
[36] D. P. Abraham, R. D. Twesten, M. Balasubramanian, I. Petrov, J. McBreen, K. Amine, *Electrochem. Commun.* **2002**, *4*, 620.
[37] S. U. Woo, C. S. Yoon, K. Amine, I. Belharouak, Y. K. Sun, *J. Electrochem. Soc.* **2007**, *154*, A1005.
[38] Y. K. Sun, B. R. Lee, H. J. Noh, H. M. Wu, S. T. Myung, K. Amine, *J. Mater. Chem.* **2011**, *21*, 10108.
[39] Y. K. Sun, Z. H. Chen, H. J. Noh, D. J. Lee, H. G. Jung, Y. Ren, S. Wang, C. S. Yoon, S. T. Myung, K. Amine, *Nat. Mater.* **2012**, *11*, 942.
[40] L. F. Cui, Y. Yang, C. M. Hsu, Y. Cui, *Nano Lett.* **2009**, *9*, 3370.
[41] J.-G. Ren, Q.-H. Wu, G. Hong, W.-J. Zhang, H. Wu, K. Amine, J. Yang, S.-T. Lee, *Energy Technol.* **2013**, *1*, 77.
[42] L. Ji, H. Zheng, A. Ismach, Z. Tan, S. Xun, E. Lin, V. Battaglia, V. Srinivasan, Y. Zhang, *Nano Energy* **2012**, *1*, 164.
[43] S. Stankovich, D. A. Dikin, R. D. Piner, K. A. Kohlhaas, A. Kleinhammes, Y. Jia, Y. Wu, S. T. Nguyen, R. S. Ruoff, *Carbon* **2007**, *45*, 1558.
[44] J. I. Paredes, S. Villar-Rodil, A. Martinez-Alonso, J. M. D. Tascon, *Langmuir* **2008**, *24*, 10560.
[45] T. Yoon, M. Cho, Y. W. Suh, E. S. Oh, J. K. Lee, *J. Nanosci. Nanotechnol.* **2011**, *11*, 10193.
[46] R. Yi, F. Dai, M. L. Gordin, H. Sohn, D. Wang, *Adv. Energy Mater.* **2013**, DOI: 10.1002/aenm.201300496.
[47] H.-J. Noh, Z. Chen, C. S. Yoon, J. Lu, K. Amine, Y.-K. Sun, *Chem. Mater.* **2013**, *25*, 2109.
[48] M. H. Ryou, G. B. Han, Y. M. Lee, J. N. Lee, D. J. Lee, Y. O. Yoon, J. K. Park, *Electrochim. Acta* **2010**, *55*, 2073.
[49] L. X. Liao, X. Q. Cheng, Y. L. Ma, P. J. Zuo, W. Fang, G. P. Yin, Y. Z. Gao, *Electrochim. Acta* **2013**, *87*, 466.
[50] N. I. Kovtyukhova, P. J. Ollivier, B. R. Martin, T. E. Mallouk, S. A. Chizhik, E. V. Buzaneva, A. D. Gorchinskiy, *Chem. Mater.* **1999**, *11*, 771.